The EMBO Journal (2012) 31, 3442–3456 | © 2012 European Molecular Biology Organization | Some Rights Reserved 0261-4189/12
www.embojournal.org

THE EMBO JOURNAL

EMBO open

Modulation of synaptic function by VAC14, a protein that regulates the phosphoinositides PI(3,5)P_2 and PI(5)P

Yanling Zhang[1,2,7], Amber J McCartney[3,4,7], Sergey N Zolov[1,2], Cole J Ferguson[3,5], Miriam H Meisler[5], Michael A Sutton[4,6,*] and Lois S Weisman[1,2,*]

[1]Department of Cell and Developmental Biology, University of Michigan, Ann Arbor, MI, USA, [2]Life Sciences Institute, University of Michigan, Ann Arbor, MI, USA, [3]Neuroscience Graduate Program, University of Michigan, Ann Arbor, MI, USA, [4]Molecular and Behavioral Neuroscience Institute, University of Michigan, Ann Arbor, MI, USA, [5]Department of Human Genetics, University of Michigan, Ann Arbor, MI, USA and [6]Department of Molecular and Integrative Physiology, University of Michigan, Ann Arbor, MI, USA

Normal steady-state levels of the signalling lipids PI(3,5)P_2 and PI(5)P require the lipid kinase FAB1/PIKfyve and its regulators, VAC14 and FIG4. Mutations in the PIKfyve/VAC14/FIG4 pathway are associated with Charcot-Marie-Tooth syndrome and amyotrophic lateral sclerosis in humans, and profound neurodegeneration in mice. Hence, tight regulation of this pathway is critical for neural function. Here, we examine the localization and physiological role of VAC14 in neurons. We report that endogenous VAC14 localizes to endocytic organelles in fibroblasts and neurons. Unexpectedly, VAC14 exhibits a pronounced synaptic localization in hippocampal neurons, suggesting a role in regulating synaptic function. Indeed, the amplitude of miniature excitatory postsynaptic currents is enhanced in both *Vac14*$^{-/-}$ and *Fig4*$^{-/-}$ neurons. Re-introduction of VAC14 in postsynaptic *Vac14*$^{-/-}$ cells reverses this effect. These changes in synaptic strength in *Vac14*$^{-/-}$ neurons are associated with enhanced surface levels of the AMPA-type glutamate receptor subunit GluA2, an effect that is due to diminished regulated endocytosis of AMPA receptors. Thus, VAC14, PI(3,5)P_2 and/or PI(5)P play a role in controlling postsynaptic function via regulation of endocytic cycling of AMPA receptors.

The EMBO Journal (2012) **31,** 3442–3456. doi:10.1038/emboj.2012.200; Published online 27 July 2012
Subject Categories: membranes & transport; neuroscience
Keywords: AMPA receptor; PIKfyve; phosphatidylinositol 3,5-bisphosphate; PtdIns(3,5)P_2; synapse

*Corresponding authors. MA Sutton, Molecular and Behavioral Neuroscience Institute, University of Michigan, 5067 BSRB, 109 Zina Pitcher Place, Ann Arbor, MI 48109-2200, USA. Tel.: +1 734 615 2445; Fax: +1 734 936 3690; E-mail: masutton@umich.edu or LS Weisman, Life Sciences Institute, The University of Michigan, 210 Washtenaw Avenue, Room 6437, Ann Arbor, MI 48109-2216, USA. Tel.: +1 734 647 2537; Fax: +1 734 615 5493; E-mail: lweisman@umich.edu
[7]These authors contributed equally to this work

Received: 13 September 2011; accepted: 28 June 2012; published online: 27 July 2012

Introduction

Phosphorylated phosphoinositide (PI) lipids reside on the cytoplasmic side of eukaryotic membranes and regulate a diverse array of cellular functions. The sn-3, 4 and 5 positions of the inositol head group have the potential to be phosphorylated in all seven combinations and each type of PI plays unique roles in mammals. Each PI recruits a distinct set of protein effectors and regulates multiple cellular events including membrane traffic (Corvera *et al*, 1999; Roth, 2004), protein sorting (Saksena *et al*, 2007), growth factor signalling (Cantley, 2002), ion homeostasis (Balla, 2006; Dong *et al*, 2010), cell survival (Brunet *et al*, 2001) and cell motility (Yin and Janmey, 2003).

PI lipids are tightly regulated and inter-converted by an array of lipid kinases and phosphatases. A conserved protein complex including PIKfyve/FAB1/PIP5K3 (GenBank accession # NP_035216), VAC14 (NP_666328) and FIG4/SAC3 (NP_598760) is responsible for the biosynthesis and turnover of PI(3,5)P_2 (Jin *et al*, 2008; Ikonomov *et al*, 2009). PIKfyve is the PI(3)P 5-kinase that phosphorylates PI(3)P to form PI(3,5)P_2 (Gary *et al*, 1998), whereas FIG4 dephosphorylates PI(3,5)P_2 back to PI(3)P (Rudge *et al*, 2004; Duex *et al*, 2006a). The presence of both a kinase and a phosphatase in the same complex allows for tight regulation of PI(3,5)P_2 levels. VAC14, a HEAT repeat protein, forms a scaffold for formation of the complex and also brings in other regulatory factors (Jin *et al*, 2008). Loss of PIKfyve or VAC14 causes a loss or decrease in PI(3,5)P_2 levels, respectively (Duex *et al*, 2006b; Zhang *et al*, 2007; Ikonomov *et al*, 2011). While knockout of FIG4 might be predicted to increase PI(3,5)P_2, FIG4 also activates PIKfyve and thus, PI(3,5)P_2 is decreased in *Fig4*$^{-/-}$ fibroblasts (Chow *et al*, 2007) and yeast (Duex *et al*, 2006a). Interestingly, impairment of PIKfyve activity by either loss of VAC14 (Zhang *et al*, 2007) or pharmacological inhibition with YM201636 (Sbrissa *et al*, 2012) also causes a decrease in PI(5)P levels in mammalian cells. Note that the yeast *S. cerevisiae* does not produce PI(5)P. In mammals, the PI(5)P pool could come either from direct phosphorylation of phosphatidylinositol by PIKfyve (Sbrissa *et al*, 1999), or via dephosphorylation of PI(3,5)P_2 by myotubularin family phosphatases (Tronchère *et al*, 2004); both pathways are dependent on PIKfyve activity.

The PIKfyve/VAC14/FIG4 complex is critical for endomembrane homeostasis and has been implicated in an ever-growing list of processes. In yeast, PI(3,5)P_2 regulates vacuole fission, vacuole acidification (Bonangelino *et al*, 1997, 2002; Gary *et al*, 1998), retrograde traffic from the vacuole (Bryant *et al*, 1998; Dove *et al*, 2004) and is involved in the assembly of transcriptional regulators (Han and Emr, 2011). In metazoans, the PIKfyve/VAC14/FIG4 pathway regulates endosome-to-trans-Golgi network retrograde transport (Rutherford *et al*, 2006), autophagy (Rusten *et al*, 2007;

de Lartigue *et al*, 2009; Ferguson *et al*, 2009), exocytosis (Osborne *et al*, 2008), calcium channel activation (Shen *et al*, 2009; Dong *et al*, 2010) and degradation (Tsuruta *et al*, 2009). In plants, the PIKfyve/VAC14/FIG4 pathway is involved in endocytosis, vacuole formation, auxin transporter recycling, and pollen development (Hirano and Sato, 2011; Hirano *et al*, 2011). It remains to be determined which of the mammalian pathways are regulated by $PI(3,5)P_2$ and/or PI(5)P.

Analysis of several mouse mutants point to critical roles for the PIKfyve/VAC14/FIG4 pathway in the central and peripheral nervous systems. *Vac14* gene trap ($Vac14^{-/-}$) mice have half of the normal levels of $PI(3,5)P_2$ and PI(5)P. They develop normally, yet die perinatally with numerous neural defects including spongiform-like lesions and increased apoptosis in the brain, and intracellular vacuolation in peripheral neurons (Zhang *et al*, 2007). $Fig4^{-/-}$ (Chow *et al*, 2007; Ferguson *et al*, 2009; Lenk *et al*, 2011) and $Vac14^{L156R/L156R}$ (*ingls*) (Jin *et al*, 2008), mouse mutants defective in $PI(3,5)P_2$ and PI(5)P regulation, have similar patterns of neurodegeneration to that observed in the $Vac14^{-/-}$ mouse.

Importantly, human patients with minor defects in the PIKfyve/VAC14/FIG4 pathway also display severe neurological problems. Mutations in *FIG4* are responsible for human Charcot-Marie-Tooth disease type 4J (CMT4J), a recessive disorder affecting the peripheral nervous system (Chow *et al*, 2007; Nicholson *et al*, 2011). The most common CMT4J allele, I41T, destabilizes the mutant FIG4 protein and impairs its binding to VAC14 (Ikonomov *et al*, 2010; Lenk *et al*, 2011). Heterozygous *FIG4* mutations have also been identified in patients with amyotrophic lateral sclerosis (ALS) and primary lateral sclerosis (PLS), two forms of motor neuron disease (Chow *et al*, 2009). These observations suggest that the PIKfyve/VAC14/FIG4 pathway has specialized functions in the nervous system.

Defects in multiple neural cell types likely contribute to the pathologies observed in VAC14/FIG4-deficient mouse models. Both neurons (Chow *et al*, 2007; Zhang *et al*, 2007, 2008; Katona *et al*, 2011) and astrocytes (Jin *et al*, 2008; Ferguson *et al*, 2009) are affected by mutations in VAC14 or FIG4. However, expression of FIG4 in neurons, but not astrocytes, rescues the spongiform-like lesions, gliosis and early lethality in $Fig4^{-/-}$ mice (Ferguson *et al*, 2012), emphasizing the importance of the PIKfyve/VAC14/FIG4 pathway in neuronal function.

Neurons are highly polarized cells that process electrochemical signals by extending long specialized processes—axons and dendrites—to facilitate information transfer through neural circuits. Accordingly, the endosomal system in neurons has both general and specialized pathways, such as long-range trafficking along neurites (Ibáñez, 2007), as well as specialized recycling in both the presynaptic and postsynaptic terminals (Kennedy and Ehlers, 2006; Dittman and Ryan, 2009). These membrane events are critical for multiple aspects of neuronal function such as neurite outgrowth, neurotrophic factor signalling and synaptic plasticity (Lasiecka and Winckler, 2011). However, the role of PIKfyve/VAC14/FIG4 in neuronal function remains unknown.

Here, we address the functional significance of the PIKfyve/VAC14/FIG4 pathway in cultured neurons from the hippocampus of wild-type and $Vac14^{-/-}$ mice. To gain insight into the cellular distribution of PIKfyve/VAC14/FIG4 pathway, we developed an antibody to VAC14, suitable for immunofluorescence microscopy, and found that endogenous VAC14 localizes to multiple organelles, consistent with multiple roles for $PI(3,5)P_2$ in the endomembrane system. VAC14 partially colocalizes with early endosomes, late endosomes, lysosomes and autophagosomes. In neurons, VAC14 is found in both somatodendritic regions and axons. Notably, a substantial amount of endogenous VAC14 is present at synaptic sites, suggesting a role for VAC14 in the regulation of synaptic efficacy. Indeed, we find that synaptic function is altered in neurons cultured from $Vac14^{-/-}$ and $Fig4^{-/-}$ mice. Both postsynaptic function and surface expression of AMPA-type glutamate receptors are enhanced in $Vac14^{-/-}$ hippocampal neurons. Expression of VAC14 in $Vac14^{-/-}$ neurons reverses the synaptic phenotype, indicating a cell-autonomous and post-developmental role for VAC14 in regulating excitatory synaptic strength. We further show that the elevated surface AMPA receptor levels in $Vac14^{-/-}$ neurons are due to decreased endocytosis at postsynaptic sites. Together, our results identify control of $PI(3,5)P_2$ and/or PI(5)P synthesis as a novel regulatory pathway at synapses that influences surface levels of glutamate receptors and synaptic function.

Results

$Vac14^{-/-}$ hippocampal neurons exhibit vacuolation, but otherwise develop normally in culture

Consistent with its importance in the nervous system, expression of VAC14 is abundant in the brain relative to other tissues (Supplementary Figure S1A and B). In this study, we sought insights into the neuronal-specific functions of the PIKfyve/VAC14/FIG4 complex. We focused on hippocampal neurons because VAC14 expression in the hippocampus is similar to other brain regions (Supplementary Figure S1C) and the hippocampus is largely spared from neurodegeneration, even at the time of death in $Vac14^{-/-}$ and $Fig4^{-/-}$ animals (Chow *et al*, 2007; Zhang *et al*, 2007). Hippocampal neurons from $Vac14^{-/-}$ embryos remain viable for several weeks, which enabled us to examine the impact of *Vac14* deletion in these cells.

Although no spongiform lesions were observed in hippocampal regions *in vivo*, cultured $Vac14^{-/-}$ hippocampal neurons developed small vacuoles in the soma as early as 1 day *in vitro* (DIV) (Supplementary Figure S2A). Similarly to fibroblasts, the neuronal vacuoles are positive for the late endosome/lysosome marker LAMP1 and negative for the early endosome marker EEA1 (Supplementary Figure S2B). Notably, at the neuron density used (2×10^4 per 1.91 cm^2), vacuoles are also observed in neurites by 12 DIV, suggesting that VAC14 functions in both the soma and neurites. Vacuole formation in $Vac14^{-/-}$ neurons appears to be activity independent; the degree of vacuolation in cells subjected to activity blockade (1 μM TTX, 40 μM CNQX, 20 μM APV) from DIV3 to DIV18 was similar to that in untreated neurons (Supplementary Figure S2C).

The presence of vacuoles in neurons lacking VAC14 did not appear to affect axon and dendrite development in culture, as assessed using the five stage model (Dotti *et al*, 1988; Supplementary Figure S3A). $Vac14^{-/-}$ neurons progressed

from stage I (lamellipodia) to stage IV/V (complicated networks) at a rate similar to wild-type neurons (Supplementary Figure S3B), implying normal neurite outgrowth and differentiation.

Subcellular localization of VAC14 in cultured fibroblasts

To determine the sites of action of the PIKfyve/VAC14/FIG4 complex in neurons, we determined the localization of endogenous VAC14. Previous attempts to localize components of the PIKfyve complex in non-neuronal cells relied on overexpression of tagged proteins, and have produced divergent results. An earlier study indicated that overexpressed, tagged PIKfyve is confined to late endosome/lysosome compartments (Ikonomov *et al*, 2001), whereas other analyses found tagged FAB1/PIKfyve primarily localized to early endosomes (Cabezas *et al*, 2006; Rutherford *et al*, 2006).

To better understand the endogenous cellular distribution of the PIKfyve/VAC14/FIG4 complex, we raised a rabbit polyclonal antibody against full-length human VAC14 protein. After extensive affinity purification, we obtained a reagent that, in western blot analysis, revealed a major band at the expected molecular weight (88 kD) in wild-type but not in *Vac14*$^{-/-}$ brain (Supplementary Figure S1A). In wild-type fibroblasts, permeabilized with saponin prior to fixation, VAC14 was present on punctate organelles distributed throughout the cytoplasm; these structures were absent from *Vac14*$^{-/-}$ fibroblast controls (Figure 1A). Nuclear staining was frequently observed in both wild-type and *Vac14*$^{-/-}$ cells (Supplementary Figure S4A); thus, the antibody is not suitable to test whether VAC14 is also localized in the nucleus.

To determine the relative distribution of VAC14 on endosomal and lysosomal membranes, we performed triple labelling experiments in primary fibroblasts and determined the distribution of VAC14, EEA1 and LAMP1 puncta (Figure 1B; Supplementary Figure S4B and F). Consistent with earlier studies, EEA1 and LAMP1 labelled distinct compartments. The majority of VAC14 puncta colocalized with EEA1 (20 ± 5%), LAMP1 (30 ± 5%) or both markers (19 ± 7%). These triple-labelled puncta likely represent intermediate endosomes. Thus, VAC14, PI(3,5)P_2 and potentially PI(5)P, are present in multiple locations within the endomembrane system, including early endosomes, late endosomes and lysosomes (Supplementary Figure S5). Some VAC14 puncta (31 ± 8%) did not colocalize with either EEA1 or LAMP1, suggesting that VAC14 may also function on other compartments.

LAMP1 is present on both late endosomes and lysosomes. To determine whether VAC14 is found on one or both of these compartments, we examined VAC14 localization relative to LBPA (late endosomes) or internalized dextran (lysosomes). Partial colocalization was observed between VAC14 (15 ± 6%) and LBPA (Figure 1C; Supplementary Figure S4C and G), which indicates that some VAC14 resides on late endosomes. To determine whether lysosomes also contain VAC14, cells were incubated with a fluid phase marker, 70 kD Texas Red-dextran, and then chased in the absence of dextran for 24 h to allow it to reach lysosomes. Partial colocalization was observed between VAC14 (23 ± 9%) and lysosomes loaded with dextran (Figure 1D; Supplementary Figure S4D and G), suggesting that some VAC14 is also localized on lysosomes. Interestingly, the limiting membrane of vacuoles in *Vac14*$^{-/-}$ fibroblasts is positive for LAMP1, but negative for LBPA (Figure 1E), implying that the large vacuoles derive solely from lysosomes.

In metazoans, the PIKfyve/VAC14/FIG4 pathway is thought to play a role in autophagy, either during fusion of autophagosomes with endosomes/lysosomes, or recycling of lysosomes from autolysosomes (Rusten *et al*, 2007; de Lartigue *et al*, 2009; Ferguson *et al*, 2009). LC3 is a common marker of autophagosomes. We transfected wild-type or *Vac14*$^{-/-}$ fibroblasts with LC3-RFP and colabelled transfected cells with anti-VAC14. VAC14 (17 ± 13%) partially colocalized with LC3 (Figure 1F; Supplementary Figure S4E and G), suggesting that autophagosomes may contain PI(3,5)P_2 and/or PI(5)P. Alternatively, these PI(3,5)P_2 and/or PI(5)P containing regions may represent the interface between autophagosomes and endosomes/lysosomes.

Localization of VAC14 in neurons

To determine the localization of VAC14 in neurons, we first examined its distribution in the soma. In this case, neurons were not permeabilized with saponin prior to fixation; thus, the images indicate both membrane bound and cytosolic pools of VAC14. A significant portion of the VAC14 localized to punctate structures (Supplementary Figure S6). As in fibroblasts, VAC14 puncta colocalized both with the early endosome marker, EEA1 (Supplementary Figure S6A), and with the late endosome/lysosome marker, LAMP2 (Supplementary Figure S6B).

To test whether VAC14 is present in dendrites, hippocampal neurons were labelled with antibodies against VAC14 and against MAP2, a microtubule-associated protein that is highly expressed in dendrites but not in axons. Notably, discrete VAC14 puncta were found in MAP2-positive dendrites (Figure 2A; Supplementary Figure S7A). Moreover, another pool of VAC14 puncta was evident in MAP2-negative neurites, implying an axonal localization. To test this further, we labelled neurons with anti-VAC14 and anti-TAU-1, which preferentially labels axons in younger cultures (Horton *et al*, 2005). Again, VAC14 puncta were present in TAU-1-labelled axons (Figure 2A; Supplementary Figure S7A), although this axonal VAC14 pool was less prominent than the dendritic pool. In neurites, VAC14 puncta partially colocalized with both EEA1 (23 ± 12%) and LAMP1 (29 ± 9%) (Figure 2B; Supplementary Figure S7B and C), suggesting that VAC14 in neuronal processes functions in pathways that involve early and late endosomes as well as lysosomes.

Endogenous VAC14 localizes to synapses

Interestingly, the most striking colocalization was observed between VAC14 and synaptic markers. A substantial number of VAC14 puncta colocalized with the presynaptic terminal markers synapsin, synaptotagmin and VAMP/synaptobrevin (Figure 2C; Supplementary Figure S7D). To test whether VAC14 colocalizes with excitatory synapses, we performed triple labelling against VAC14, vGlut1 (the glutamate transporter on presynaptic vesicles), and the postsynaptic scaffolding protein PSD95. VAC14 puncta colocalized extensively with vGlut1/PSD95 double-positive puncta (Figure 2D; Supplementary Figure S7E), suggesting a role for VAC14 in excitatory synapse function.

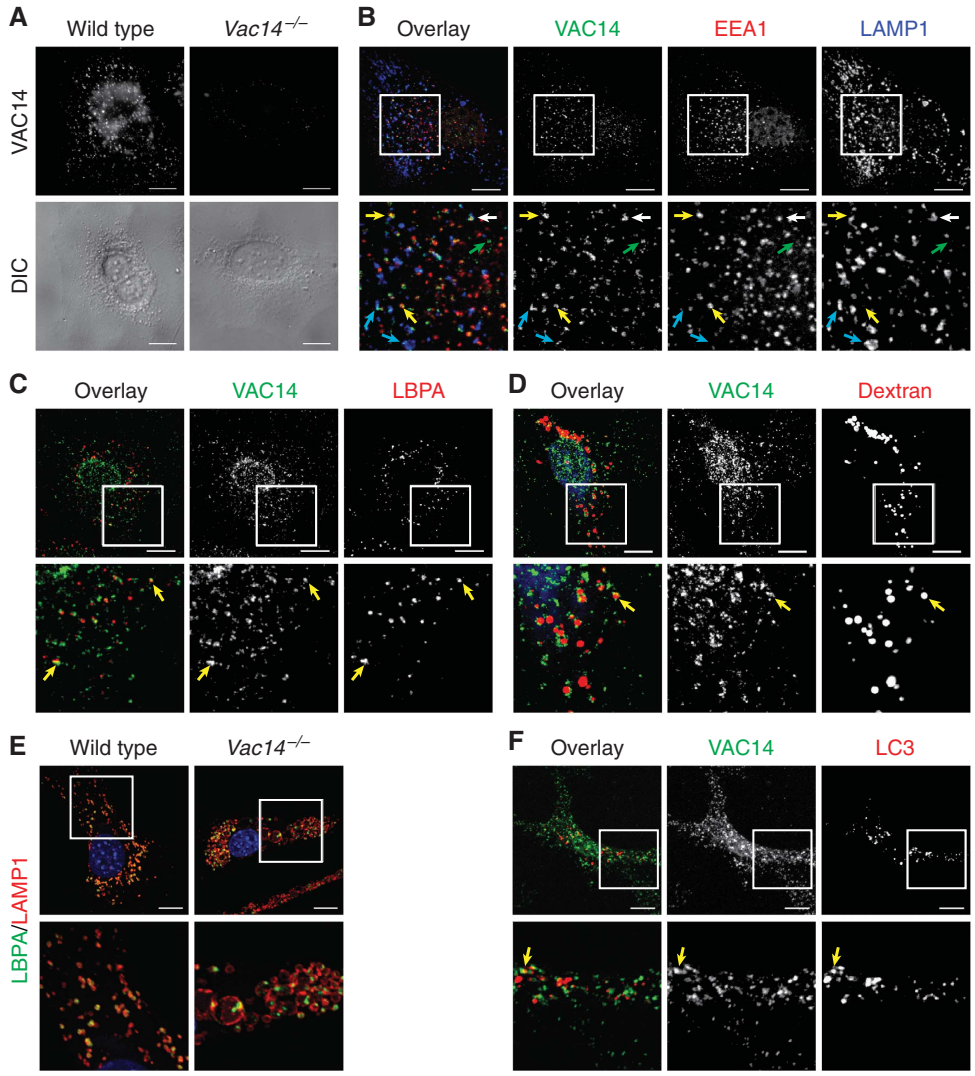

Figure 1 Endogenous VAC14 partially colocalizes with multiple endocytic organelles. (**A**) Polyclonal VAC14 antibody recognizes punctate structures in wild-type cells. Fibroblasts were permeabilized with saponin followed by fixation, then labelled with anti-VAC14 antibody. Bottom panels, DIC images. (**B**) In fibroblasts, endogenous VAC14 colocalizes with both EEA1 and LAMP1. Wild-type fibroblasts were triple labelled with rabbit anti-VAC14, chicken anti-EEA1 and rat anti-LAMP1. The majority of VAC14 colocalized with either EEA1 (yellow arrows) or LAMP1 (turquoise arrows). Some VAC14 colocalized with both (white arrows) or neither (green arrow) markers. (**C**) VAC14 partially colocalizes with the late endosome marker LBPA (arrow). Fibroblasts were double labelled with rabbit anti-VAC14 and mouse anti-LBPA. (**D**) VAC14 partially colocalized with lysosomes (arrow). To label lysosomes, prior to fixation, fibroblasts were pulsed with Texas Red-Dextran (Mw 70 kD) for 1 h and chased in the absence of dextran for 24 h. (**E**) The limiting membrane of vacuoles in *Vac14*$^{-/-}$ cells is positive for LAMP1 while negative for LBPA, suggesting a lysosomal origin. *Vac14*$^{-/-}$ fibroblasts were double labelled with rat anti-LAMP1 and mouse anti-LBPA. (**D**, **E**) DAPI (blue) used to label nuclei. (**F**) VAC14 partially colocalizes with LC3-RFP puncta (arrows). Fibroblasts transfected with LC3-RFP were fixed and labelled with anti-VAC14. (**A**–**F**) Bar = 10 μm.

Altered synaptic function in cultured Vac14*$^{-/-}$ *neurons

To examine a functional role for the PIKfyve/VAC14/FIG4 pathway at the synapse, we measured miniature excitatory postsynaptic currents (mEPSCs) in pyramidal-like neurons from *Vac14*$^{-/-}$ hippocampal cultures and corresponding wild-type controls. mEPSCs represent unitary synaptic currents mediated by the spontaneous fusion of single synaptic vesicles, and are often used to reveal functional changes in synaptic strength. Pyramidal-like neurons with little to no vacuolation were targeted for electrophysiology. Given the neurodegeneration observed in other regions of the brain at the time of birth, one might expect synaptic function to be diminished in *Vac14*$^{-/-}$ neurons. Surprisingly, mEPSCs from *Vac14*$^{-/-}$ neurons displayed a significant increase (24 ± 6%) in amplitude relative to wild-type mEPSCs (Figure 3A and B), suggesting an inhibitory role for VAC14 in synaptic function. We found no difference in mEPSC frequency or decay time in *Vac14*$^{-/-}$ mEPSCs (Figure 3C–E). In a parallel experiment, we found mEPSC amplitude was similarly increased in *Fig4*$^{-/-}$ mice (Figure 3F and G), which also have reduced PIKfyve kinase activity. Together, these data suggest that the increase in mEPSC amplitude in both *Vac14*$^{-/-}$ and *Fig4*$^{-/-}$ neurons results from defects in PI(3,5)P_2 and/or PI(5)P synthesis.

Although we found no change in mEPSC frequency in either *Vac14*$^{-/-}$ (Figure 3C) or *Fig4*$^{-/-}$ neurons (Figure 3H), VAC14 is localized to axons (Figure 2A), and therefore, is well positioned to contribute to presynaptic

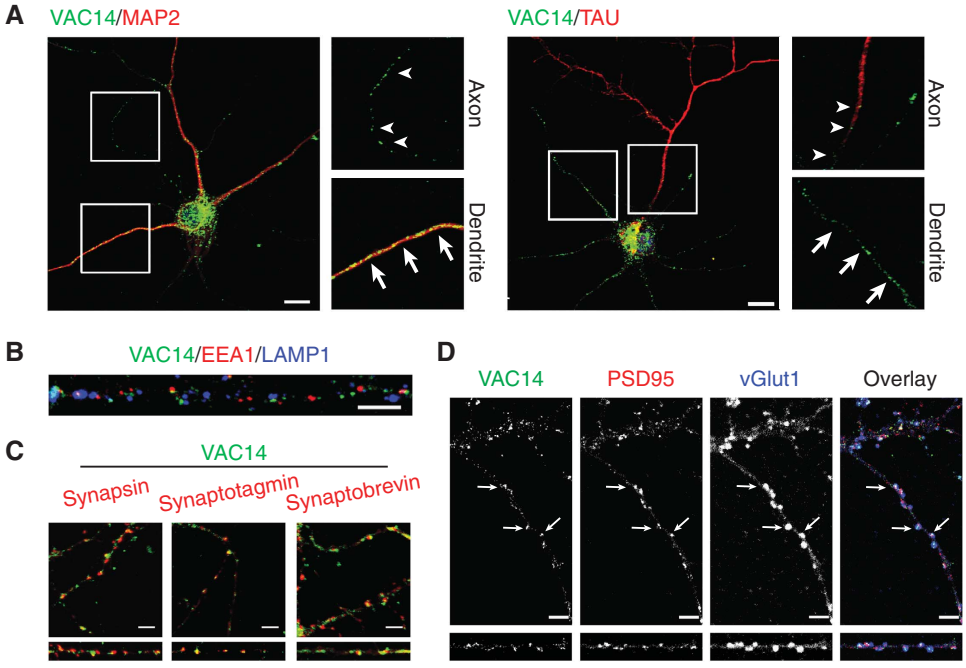

Figure 2 VAC14 is found in both dendrites and axons, and colocalizes with endocytic and synaptic markers in hippocampal neurons. (**A**) Wild-type and *Vac14*$^{-/-}$ neurons were double labelled with rabbit anti-VAC14 and mouse anti-MAP2 (dendrites) or mouse anti-TAU-1 (axons). Arrows indicate the localization of VAC14 on dendrites (MAP2-positive and TAU-negative neurites). Arrowheads indicate the localization of VAC14 on axons (MAP2-negative and TAU-1-positive neurites). Bar = 10 μm. (**B**) VAC14 partially colocalizes with EEA1 or LAMP1 in the neurites (arrows). Wild-type and *Vac14*$^{-/-}$ neurons were triple labelled with rabbit anti-VAC14, chicken anti-EEA1 and rat anti-LAMP1. Bar = 5 μm. (**C**) VAC14 displays significant colocalization with several synaptic markers: synapsin, synaptotagmin and synaptobrevin. Wild-type and *Vac14*$^{-/-}$ neurons were double labelled with rabbit anti-VAC14 and guinea pig anti-synapsin, mouse anti-synaptotagmin or mouse anti-synaptobrevin. Bar = 5 μm. (**D**) VAC14 partially localizes at excitatory synapses (labelled with both the synaptic vesicle glutamate transporter vGlut1 and postsynaptic marker PSD95). Wild-type and *Vac14*$^{-/-}$ neurons were labelled with rabbit anti-VAC14, mouse anti-PSD95 and guinea pig anti-vGlut1. Arrows indicate examples of colocalization. (**C**, **D**) Lower panels show straightened dendrites from corresponding top panels. Bar = 5 μm.

function. The enlargement of endocytic compartments in *Vac14*$^{-/-}$ cells (Zhang *et al*, 2007) also suggested that the increase in mEPSC amplitude in *Vac14*$^{-/-}$ neurons could have resulted from increased glutamate release by enlarged presynaptic vesicles (increased quantal content). To examine this possibility, we performed transmission electron microscopy on thin sections from the hippocampus and hindbrain of wild-type and *Vac14*$^{-/-}$ mice at P0. The hindbrain was included in these studies because it is the most vacuolated brain region in the *Vac14*$^{-/-}$ animal at the time of death. We found similar synaptic vesicle diameter in wild-type and *Vac14*$^{-/-}$ presynaptic terminals of both brain regions (Figure 4A and B).

Despite similar mEPSC frequency between *Vac14*$^{-/-}$ and wild-type neurons, we observed that the number of excitatory synapses in the first 100 μm of *Vac14*$^{-/-}$ dendrites was modestly but significantly decreased (Figure 4C and D). This discrepancy raised the possibility that although *Vac14*$^{-/-}$ neurons have fewer presynaptic inputs, the terminals may have elevated neurotransmitter release probability. To further examine presynaptic function, we measured the probability of synaptic vesicle release by recording postsynaptic NMDA receptor mediated currents in the presence of the use-dependent NMDA receptor antagonist, MK801 (Huettner and Bean, 1988). The degree of blockade is proportional to the number of presynaptic vesicles that release glutamate in response to stimulation (Rosenmund *et al*, 1993). We found that *Vac14*$^{-/-}$ neurons showed greater blockade than wild-type neurons (Figure 4E and F) which suggests an enhancement of release probability in *Vac14*$^{-/-}$ neurons. Given that the frequency of mEPSCs was similar, the expected change in mEPSC frequency was likely masked by the decrease in synapse number. Together, these results suggest that the PIKfyve/VAC14/FIG4 pathway modulates neurotransmitter release at the presynaptic terminal.

VAC14 levels are higher in dendrites than axons. To test whether increased mEPSC amplitude in *Vac14*$^{-/-}$ neurons is due to loss of VAC14 in the postsynaptic neuron, we transfected neurons with plasmids encoding Citrine-tagged human VAC14. For these experiments, we used calcium phosphate-based transfection because the low transfection efficiency (~1% of cells) ensures that the few neurons that express VAC14 in *Vac14*$^{-/-}$ cultures received the excitatory synaptic contacts from neurons that lack VAC14. Thus, mEPSCs recorded from transfected neurons measure the effect of restoring VAC14 to the postsynaptic cell. We found VAC14 expression reversed the increase in mEPSC amplitude observed in *Vac14*$^{-/-}$ relative to wild-type neurons, whereas expression of Citrine alone did not (Figure 5). Moreover, even in wild-type neurons, overexpression of Citrine-VAC14 significantly depressed mEPSC amplitude relative to expression of untransfected neighbours, suggesting that synaptic strength is bidirectionally regulated by the levels of VAC14 in postsynaptic neurons. Together, these results strongly implicate VAC14 in the regulation of postsynaptic function.

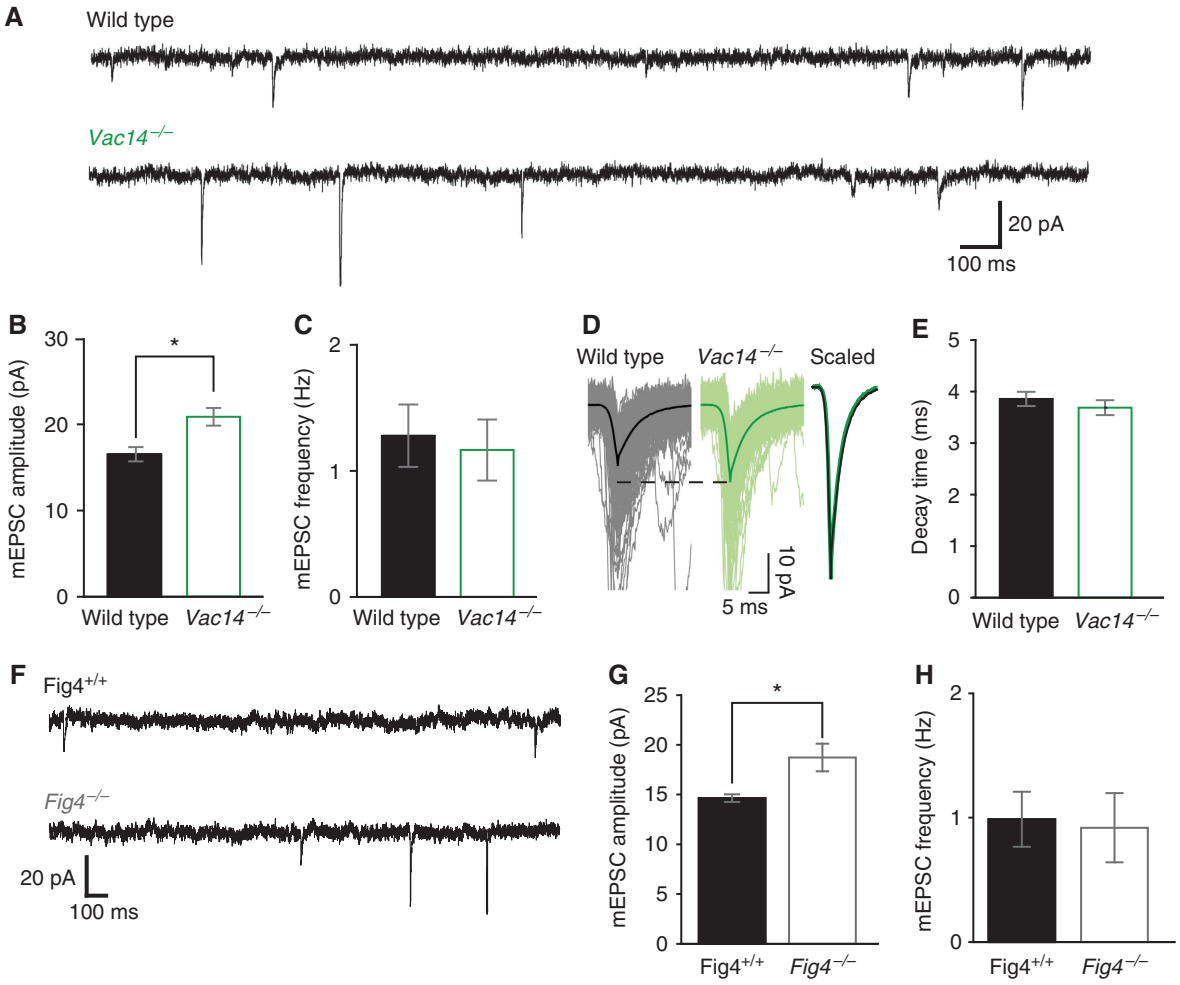

Figure 3 Loss of VAC14 or FIG4 leads to an increase in excitatory synaptic function. (**A**) Representative mEPSC recordings of wild-type ($N=32$) and *Vac14*$^{-/-}$ neurons ($N=32$). (**B**) Mean mEPSC amplitude in *Vac14*$^{-/-}$ neurons is larger than in wild-type neurons, 20.86 ± 1.03 pA versus 16.83 ± 0.91 pA, respectively. *$P=0.0045$, *t*-test. (**C**) Mean mEPSC frequency is similar in wild-type (1.21 ± 0.26 Hz) and *Vac14*$^{-/-}$ (1.16 ± 0.24 Hz) neurons. (**D**, **E**) Summary of mEPSC kinetics in wild-type and *Vac14*$^{-/-}$ neurons. (**D**) Individual mEPSCs overlaid. Thick lines show the mean trace. Dashed line is aligned to the mean peak inward current of *Vac14*$^{-/-}$ mEPSC. Scaled overlay shows similar kinetics between wild-type and *Vac14*$^{-/-}$ mEPSCs. (**E**) Mean mEPSC decay is similar between wild type (3.80 ± 0.15 ms) and *Vac14*$^{-/-}$ (3.69 ± 0.14 ms). (**F**) Representative mEPSC traces of wild-type (Fig4$^{+/+}$) ($N=12$) and *Fig4*$^{-/-}$ neurons ($N=14$). (**G**) Mean mEPSC amplitude in *Fig4*$^{-/-}$ neurons is larger than in Fig4$^{+/+}$ neurons (14.64 ± 0.39 pA versus 18.73 ± 1.38 pA, respectively, *$P=0.0164$, *t*-test). (**H**) Mean mEPSC frequency is similar in Fig4$^{+/+}$ and *Fig4*$^{-/-}$ (0.99 ± 0.22 Hz versus 0.92 ± 0.28 Hz, respectively, $P=0.8542$, *t*-test). Error bars are standard error of the mean (s.e.m.).

Surface AMPA receptors are elevated in Vac14$^{-/-}$ *hippocampal neurons*

mEPSCs are dominated by currents through AMPARs localized on the postsynaptic membrane (Gong and De Camilli, 2008). Thus, the increase in mEPSC amplitude in *Vac14*$^{-/-}$ neurons could result from changes in the number of surface AMPA receptors. Under basal conditions, most AMPA receptors in the hippocampus are heterotetramers of the GluA2 and GluA1 subunits (Lu *et al*, 2009). By western blot, we found similar levels of total GluA2 between wild-type and *Vac14*$^{-/-}$ neurons (Supplementary Figure S8). To test if the level of GluA2 at the cell surface was different, intact cultured neurons were incubated with an antibody against an extracellular epitope of GluA2 (Mouse IgG2a, MAB397; Chemicon), followed by fixation and incubation with a fluorescent secondary antibody under non-permeabilizing conditions. Surface GluA2 puncta were quantified using immunofluorescence microscopy (Figure 6A). In both wild-type and *Vac14*$^{-/-}$ neurons, there was a wide range in intensities of surface GluA2 puncta. However, in *Vac14*$^{-/-}$ neurons, the average and median surface GluA2 intensities were 34 and 17% higher, respectively, relative to wild-type neurons. The medians differed significantly with 95% confidence, indicated by the non-overlapping notches surrounding the medians in the box plot. Moreover, the cumulative distribution of surface GluA2 puncta intensities was right-shifted in *Vac14*$^{-/-}$ neurons (Figure 6B). These data indicate that surface GluA2 levels are increased in *Vac14*$^{-/-}$ neurons, which likely accounts for the increased amplitude of mEPSCs. In an independent approach, we measured the ratio of surface to total GluA2 in dendrites. Surface GluA2 was labelled as described above. Then neurons were permeabilized and labelled with a C-terminal GluA2 antibody (Rabbit pAb, AB1768; Chemicon) to identify total GluA2. We found that the ratio of surface to total GluA2 was increased in *Vac14*$^{-/-}$ dendrites, relative to wild type (Figure 6C and D). Together, these results

suggest that GluA2 receptors are expressed in *Vac14*$^{-/-}$ neurons at similar levels, but accumulate on the surface.

Trafficking of AMPA receptors is altered in Vac14$^{-/-}$ *neurons*

GluA2 undergoes constant cycling between the surface and internal pools; once internalized, GluA2 may either be degraded in lysosomes or recycled back to the plasma membrane. Perturbations in endocytosis, recycling or degradation could lead to an accumulation of surface receptors in *Vac14*$^{-/-}$ neurons. To measure the rate of endocytosis of AMPA receptors, we performed live labelling of surface GluA2 with anti-GluA2 antibody and then stimulated endocytosis via addition of NMDA (Figure 7A). After 10 min, surface bound GluA2 antibodies were stripped by a brief wash in low pH solution, such that only internalized GluA2 antibodies were detected after fixation and permeablization. Leupeptin was present throughout to prevent lysosomal

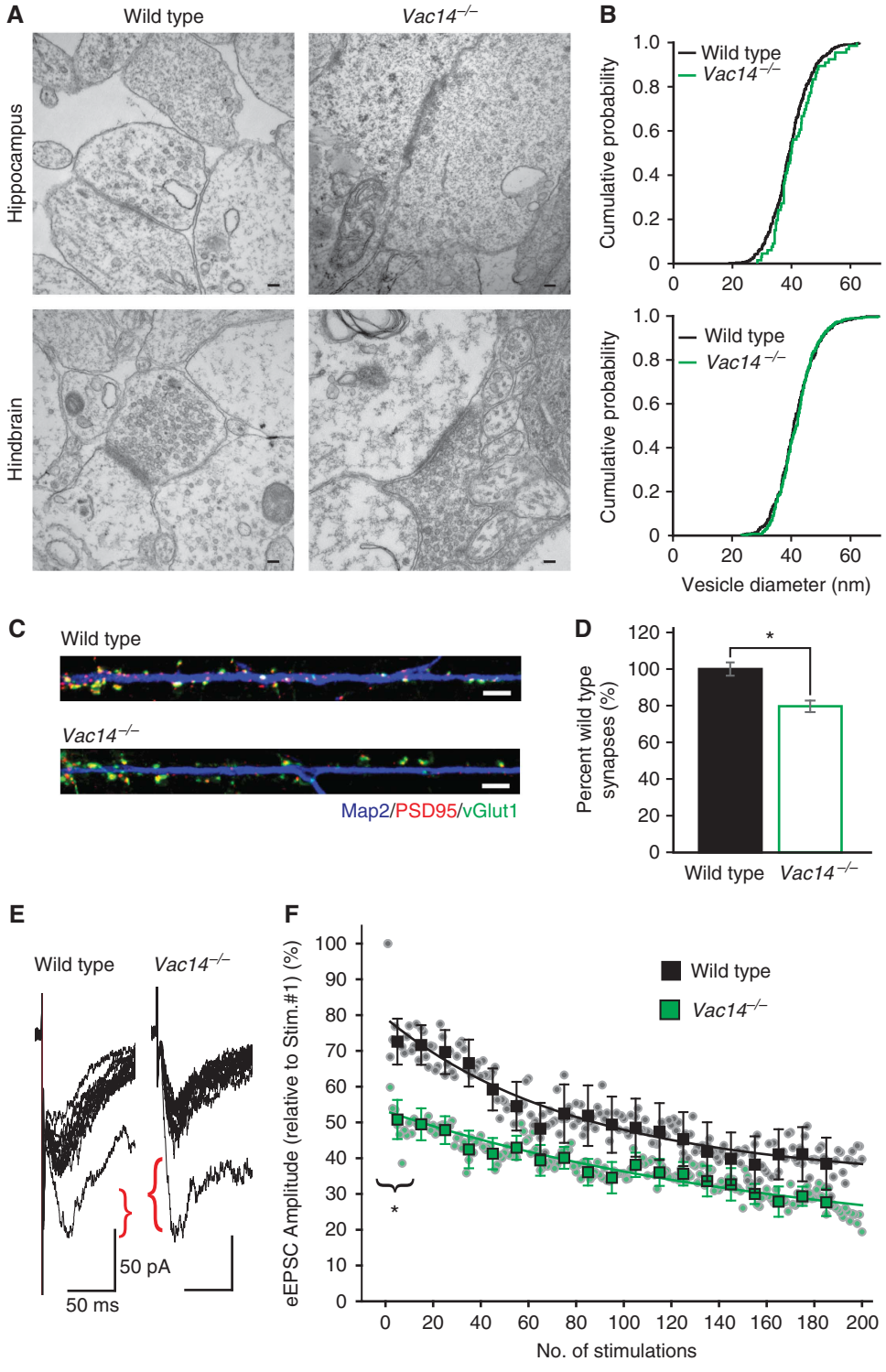

degradation. Notably, the number of internalized GluA2 puncta was decreased by 30% in dendrites in *Vac14*$^{-/-}$ neurons (Figure 7B and E). Total levels of internalized GluA2 puncta in the soma and dendrites were reduced to 71 and 56%, respectively, compared to wild type (Figure 7C and D). These results are consistent with an endocytosis defect in *Vac14*$^{-/-}$ neurons. To determine whether internalized GluA2 still enters the degradation pathway in *Vac14*$^{-/-}$ neurons, we further measured the proportion of internalized GluA2 puncta that colocalized with the late endosomal and lysosomal marker LAMP1 (Supplementary Figure S9). Though fewer internalized GluA2 puncta were observed in *Vac14*$^{-/-}$ neurons, a similar proportion exhibited colocalization with LAMP1 (27% in wild type versus 26% in

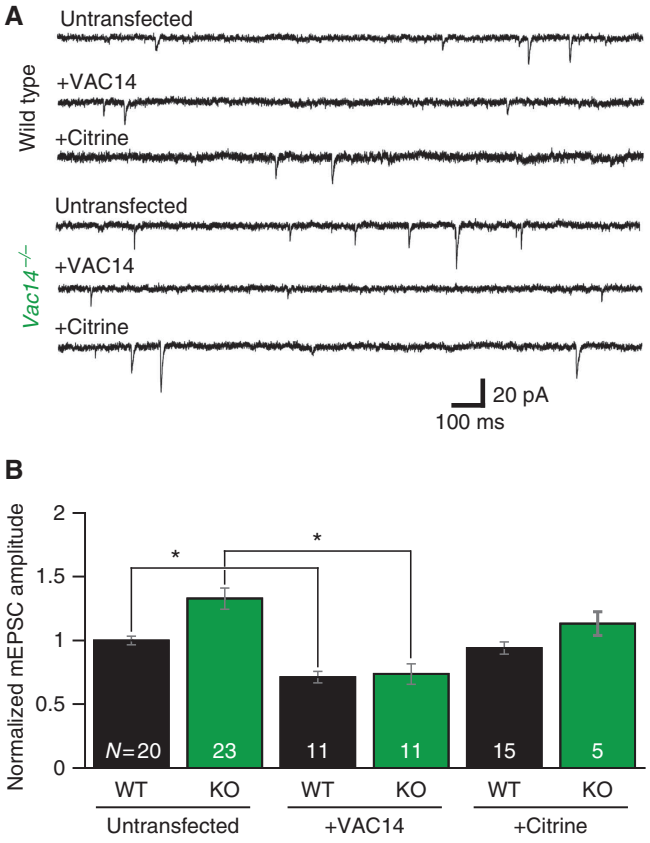

Figure 5 Restoration of VAC14 eliminates the increase in mEPSC amplitude in *Vac14*$^{-/-}$ neurons. (**A**) Examples of mEPSC recordings of wild-type and *Vac14*$^{-/-}$ neurons that were sham-transfected, expressed VAC14-Citrine or Citrine alone. (**B**) Quantification of mEPSC amplitude normalized to sham-transfected wild-type neurons shows that there is an inverse relationship between level of VAC14 expression and mEPSC amplitude. In wild-type neurons, VAC14 overexpression leads to a decrease in amplitude. The increase in mEPSC amplitude in *Vac14*$^{-/-}$ neurons is reduced by re-introduction of VAC14. Neurons transfected with Citrine were similar to untransfected wild type. One-way ANOVA test was used to compare mEPSC amplitudes ($F(5, 12.3)$, $P = 8.27 \times 10^{-9}$). *Individual comparisons between untransfected and VAC14-transfected wild-type and untransfected and VAC14-transfected *Vac14*$^{-/-}$ neurons were significant using Tukey-Kramer honestly significant difference (HSD) criterion. WT, wild type; KO, *Vac14*$^{-/-}$. Error bars, s.e.m.

Figure 4 Presynaptic probability of release is enhanced in *Vac14*$^{-/-}$ neurons. (**A**, **B**) Synaptic vesicles from *Vac14*$^{-/-}$ are not larger than synaptic vesicles observed in brains from wild type. (**A**) Electron microscopy of excitatory synapses, evident by the thickening of the postsynaptic membrane, in wild-type and *Vac14*$^{-/-}$ hippocampus and hindbrain. Bar = 100 nm. (**B**) Quantitation of the diameter of synaptic vesicles. Cumulative probability distribution of synaptic vesicle diameter. No significance difference was found between wild type and *Vac14*$^{-/-}$ by a two-sample Kolmogorov-Smirnov test (kstest2, Matlab) (hippocampus, $P = 0.32$; hindbrain, $P = 0.46$). Three wild-type and three *Vac14*$^{-/-}$ animals were analysed. Hindbrain: $N = 567$ vesicles from 33 terminals for wild type and 388 vesicles from 29 terminals for *Vac14*$^{-/-}$. Hippocampus: $N = 433$ vesicles from 33 terminals for wild type and 66 vesicles from 15 terminals for *Vac14*$^{-/-}$. (**C**, **D**) The number of synapses is decreased in *Vac14*$^{-/-}$ neurons. (**C**) Wild-type and *Vac14*$^{-/-}$ hippocampal neurons were triple labelled with rabbit anti-MAP2 (blue), mouse anti-PSD95 (red) and guinea pig anti-vGlut (green). Examples of straightened dendrites are shown. Bar = 5 μm. (**D**) Quantitation of the number of synapses on the first 100 μm of dendrites starting from the soma. The numbers of synapses were normalized to the average of wild type. *Vac14*$^{-/-}$ neurons had fewer synapses ($N = 91$ for wild type and 71 for *Vac14*$^{-/-}$) ($^*P = 1.7 \times 10^{-4}$, *t*-test). Error bars, s.e.m. (**E**, **F**) Presynaptic probability of release is increased in *Vac14*$^{-/-}$ neurons. NMDA currents were pharmacologically isolated from AMPA and $GABA_A$ mediated currents and recorded at −70 mV (solution contained zero Mg^{2+}). An extracellular stimulating electrode was placed locally and used to stimulate vesicle release in afferent axons. Once a stable response was obtained, 20 μM MK801, an open-channel blocker of NMDA receptors, was added to the bath for 5 min without stimulation. Then, 200 stimulations were delivered and amplitude of the current measured (mean amplitude is shown by filled squares). In the presence of MK-801, the current is progressively blocked. The data for each genotype were fitted with a double exponential curve. The rate of progressive blockade of NMDA current was significantly greater in *Vac14*$^{-/-}$ neurons; mean amplitude of the 2–11 stimulations is significantly lower in *Vac14*$^{-/-}$ neurons. $^*P = 0.0217$, Anova1 (Matlab).

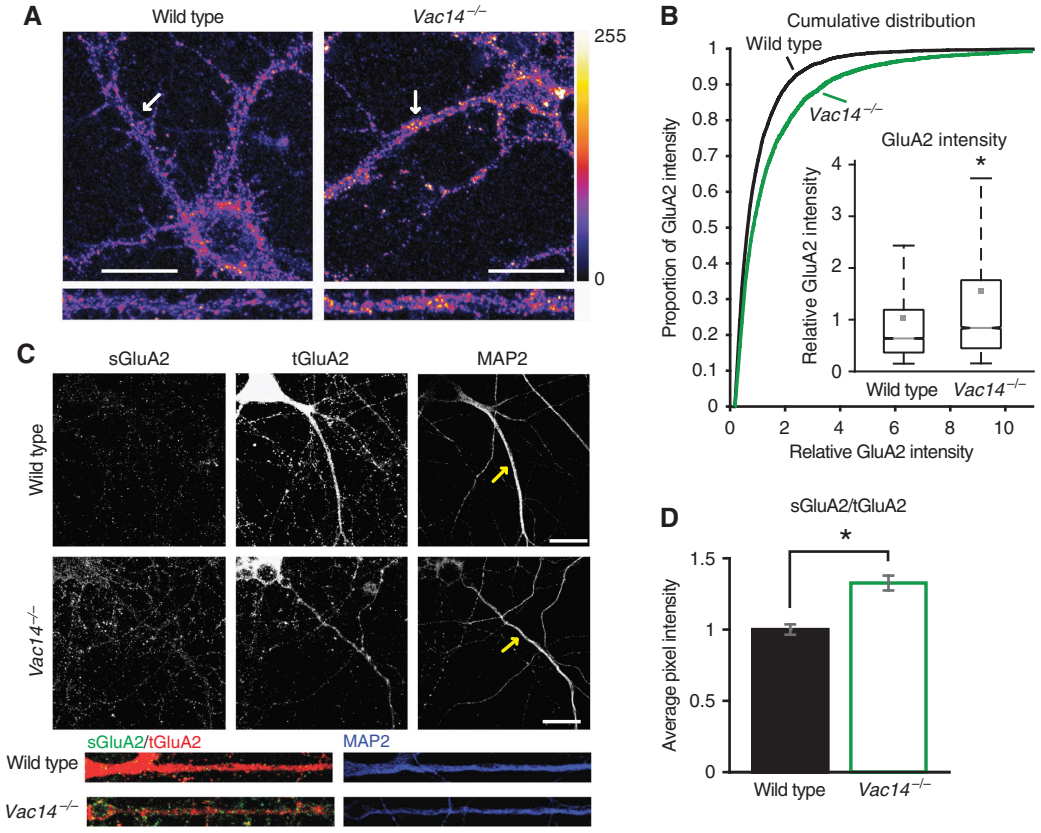

Figure 6 Surface GluA2 levels increase in *Vac14*$^{-/-}$ neurons. (**A**) Surface GluA2 was labelled by incubation of intact neurons with mouse anti-GluA2 antibody. Arrows highlight the dendrite used for analysis (enlarged in lower panels). Intensity presented in the 'fire' LUT colour scheme. (**B**) Quantitation of the intensity of GluA2 puncta, normalized to the wild-type mean. The relative intensity values from wild-type and *Vac14*$^{-/-}$ neurons are presented as a cumulative distribution. A Kolmogorov-Smirnov test demonstrates that the data sets differ significantly; $P = 1.1 \times 10^{-34}$. The median of each data set also differ significantly (box plot shown in insert). Box, interquartile range; line, median; square, mean; non-overlapping notches indicate that the two medians are statistically different at the 5% significance level; whiskers, minimum and maximum of the data within 1.5 times the length of the box. $N = 5272$ for wild type and 4756 for *Vac14*$^{-/-}$. Error bars, s.e.m. (**C**) Surface GluA2 subunits accumulate on the surface of *Vac14*$^{-/-}$ dendrites. Top three panels (wild type) and middle three panels (*Vac14*$^{-/-}$) dendrites (left to right) show surface GluA2, total GluA2, and the dendritic marker, MAP2. Yellow arrows highlight dendrites analysed. Bottom panels show the merged image of the straightened dendrite (left) and MAP2 (right). (**D**) The ratio of surface to total GluA2 is increased in *Vac14*$^{-/-}$ dendrites (1.32 ± 0.052) relative to wild type (1.0 ± 0.0364). $^{*}P = 6.836 \times 10^{-7}$, two-sample *t*-test. Scale bar = 10 μm. Error bars = s.e.m.

Vac14$^{-/-}$). This suggests that the transport of AMPA receptors late in the endocytic pathway is normal in *Vac14*$^{-/-}$ neurons. In addition, we tested whether the reduction in internalized puncta was also due to enhanced recycling back to the surface. We transfected neurons at DIV12 with plasmids encoding super-ecliptic pHluorin-tagged GluA1 (Kopec *et al*, 2006), which are strongly fluorescent when exposed to the neutral pH of the extracellular space. At DIV14, we measured the rate of internalization and recycling of pHluorin-GluA1 following NMDA stimulation (Figure 8). Five minutes of NMDA stimulation markedly reduced the intensity of pHluorin-GluA1. Following wash-out, fluorescence recovered to baseline levels as internalized receptors recycled back to the plasma membrane (Figure 8A–D). The magnitude of NMDA-dependent internalization of GluA1 was diminished in *Vac14*$^{-/-}$ neurons (Figure 8E), again suggesting reduced receptor endocytosis in these neurons. To measure the rate of recycling, we calculated the time point after NMDA stimulation at which fluorescence intensity recovered to 50% of the pre-NMDA baseline. Whereas GluA1 internalization was reduced in *Vac14*$^{-/-}$ neurons, we found no difference in the rate of recycling relative to wild type (Figure 8F). These results suggest that the initial steps in AMPA receptor endocytosis, rather than post-endocytic sorting, represent the most prominent trafficking defect accompanying loss of VAC14. Together, our findings suggest that the PIKfyve/VAC14/FIG4 pathway regulates excitatory synapse function largely via modulation of AMPA receptor endocytosis (Figure 9).

Discussion

VAC14 modulates synaptic activity in hippocampal neurons

VAC14 is present in neuronal dendrites and axons and exhibits extensive colocalization with synaptic markers. Thus, the PIKfyve/VAC14/FIG4 pathway likely impacts the synapse at multiple levels, including modulation of both presynaptic and postsynaptic function. Although here we focused on postsynaptic VAC14, our results suggest that there are also effects on presynaptic function. Thus, while mEPSC frequency is unaltered in *Vac14*$^{-/-}$ neurons, MK801 use-dependent block of NMDA receptor currents is accelerated in these cells, suggesting elevated neurotransmitter

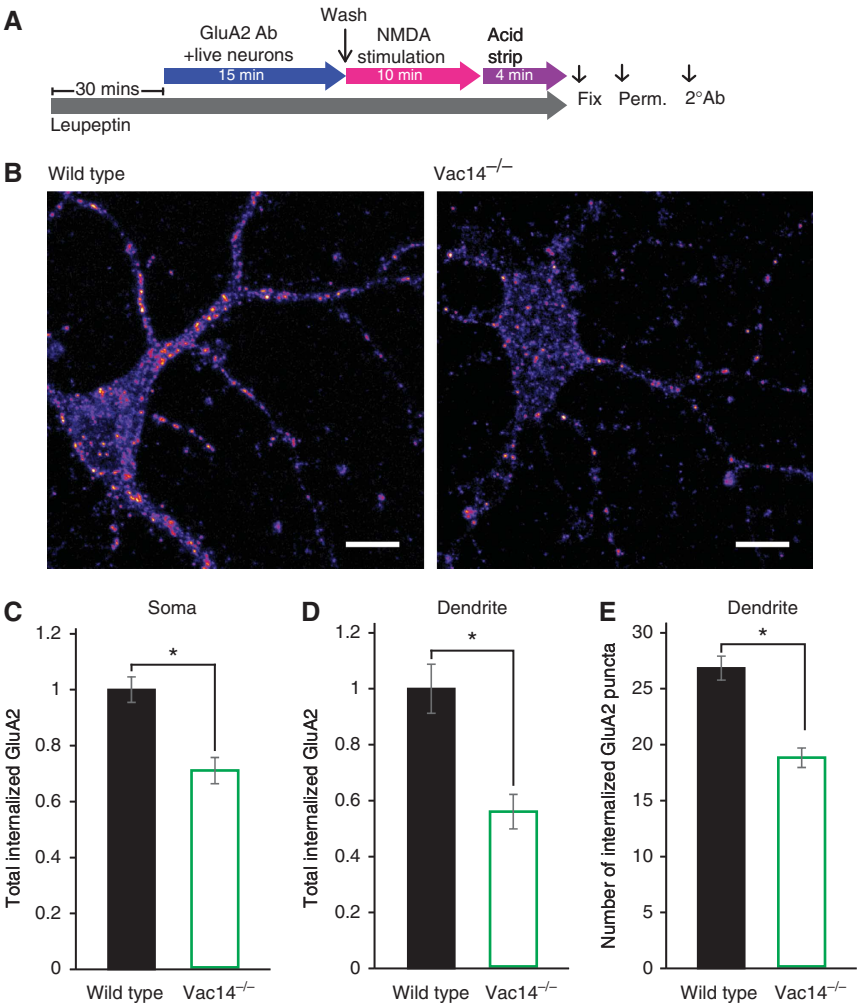

Figure 7 GluA2 endocytosis is reduced in *Vac14*$^{-/-}$ hippocampal neurons. (**A**) Diagram of experiment. Wild-type or *Vac14*$^{-/-}$ hippocampal neurons were treated with the lysosomal protease inhibitor leupeptin, then live labelled with mouse GluA2 antibodies to label those receptors exposed to the cell surface. Endocytosis was stimulated with 50 μM NMDA for 10 min. Then any remaining surface-exposed GluA2 antibody was removed with an acid wash. Neurons were then fixed and labelled with Alexa 555 anti-mouse IgG. (**B**) Example of internalized GluA2. Intensity presented in the 'fire' LUT colour scheme. Bar = 10 μm. (**C**) Total internalized GluA2 in the soma was decreased in *Vac14*$^{-/-}$ neurons ($N = 55$ for wild type and 42 for *Vac14*$^{-/-}$, $^{*}P = 2.73 \times 10^{-5}$, *t*-test). (**D**) Total internalized GluA2 in the dendrites was decreased in *Vac14*$^{-/-}$ neurons ($N = 57$ for wild type and 61 for *Vac14*$^{-/-}$, $^{*}P = 8.33 \times 10^{-5}$, *t*-test). (**E**) The number of internalized GluA2 puncta were decreased in *Vac14*$^{-/-}$ neurons ($N = 57$ for wild type and 61 for *Vac14*$^{-/-}$, $^{*}P = 5.91 \times 10^{-8}$, *t*-test). A fixed length (35 μm from the soma) was used for dendrites in (**D**) and (**E**). Error bars, s.e.m.

release probability. Consistent with a presynaptic role for PI(3,5)P_2 and/or PI(5)P, an earlier report identified *C. elegans* FIG4 at presynaptic sites in a large scale RNAi screen (Sieburth *et al*, 2005). An increase in probability of presynaptic vesicle fusion with the plasma membrane fits with a previous study demonstrating enhanced granule exocytosis following knockdown of PIKfyve in cultured chromaffin and PC12 cells (Osborne *et al*, 2008). This pathway may be interacting directly with exocytic machinery. Alternatively, it is possible that voltage-gated calcium channels or other membrane proteins that are important for membrane excitability are more highly expressed on the surface of *Vac14*$^{-/-}$ neurons, which causes increased calcium influx in response to depolarization.

The presence of VAC14, and its lipid products, in the postsynaptic terminal is consistent with earlier findings that VAC14 interacts with nNOS (Lemaire and McPherson, 2006), which interacts with the postsynaptic scaffolding protein PSD95 (Tochio *et al*, 2000). In addition, MTMR2, a phosphatase that acts on PI(3,5)P_2 *in vitro* and likely *in vivo*, also interacts with PSD95 (Lee *et al*, 2010). That VAC14 levels in the somatodendritic region are significantly higher than in axons, strongly suggested that the PIKfyve/VAC14/FIG4 pathway controls critical aspects of postsynaptic function. Indeed, we found that genetic deletion of VAC14 is accompanied by enhanced mEPSC amplitude. Importantly, postsynaptic expression of VAC14 rescues this defect, strongly suggesting that postsynaptic loss of VAC14 is responsible for the enhanced mEPSC amplitude. Moreover, *Fig4*$^{-/-}$ neurons exhibited a similar increase in mEPSC amplitude, strengthening the argument that PIKfyve/VAC14/FIG4 pathway, and their lipid products PI(3,5)P_2 and/or PI(5)P, play a role in postsynaptic function.

AMPA receptor trafficking in Vac14$^{-/-}$ *neurons*

Our results further indicate that VAC14 regulates postsynaptic function through regulation of AMPA receptor trafficking.

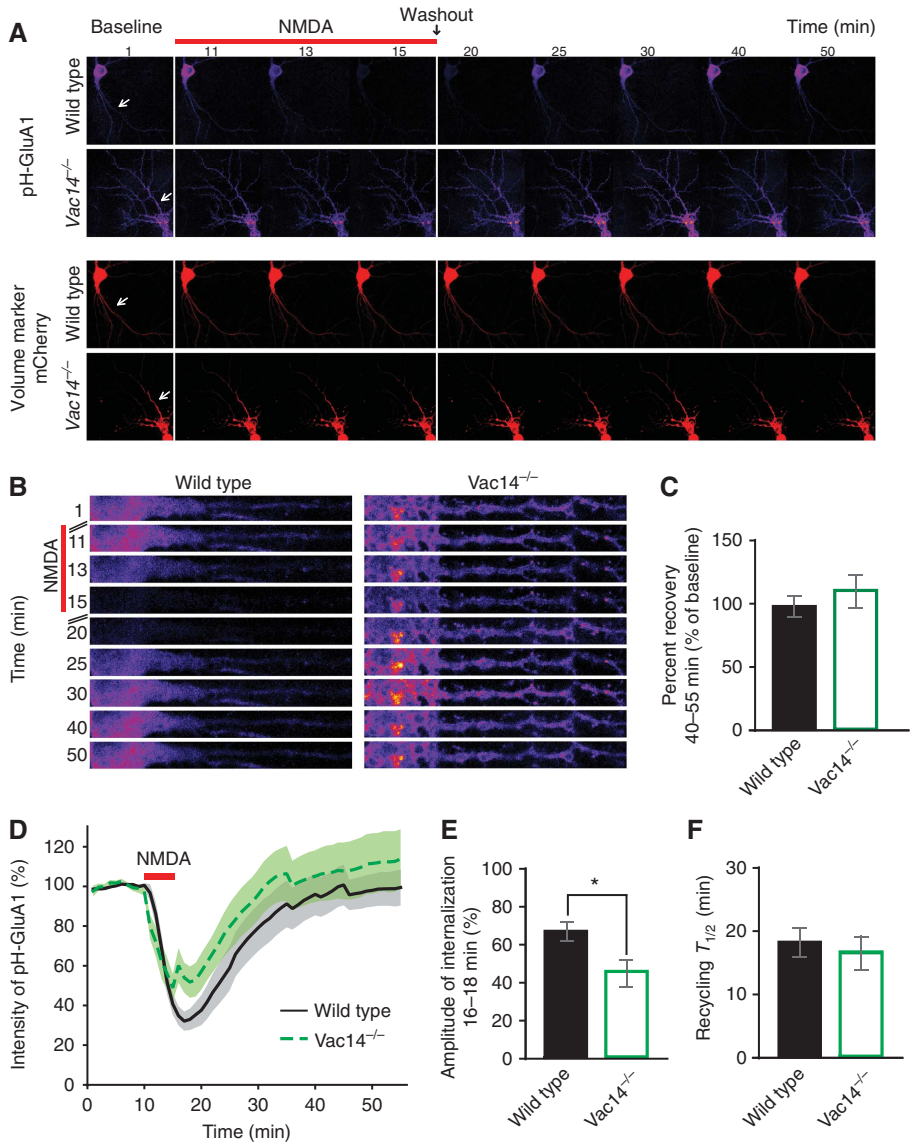

Figure 8 Endocytosis of AMPA receptors is reduced in *Vac14*$^{-/-}$ neurons. Cultured hippocampal neurons were transfected with pH-GluA1and mCherry at DIV12. At DIV14, cells were placed on the microscope stage and perfused with normal extracellular buffer. Images were acquired once per minute for a 10-min baseline, then switched to NMDA stimulation buffer for 5 min to stimulate internalization. Then, following replacement of the NMDA stimulation buffer with normal buffer, monitored for recycling back to the cell surface. The pHluorin fluorescence was imaged at 488 nm excitation, while mCherry fluorescence was imaged at 559 nm excitation, through a × 60 oil objective at a rate of one image per minute. (**A**) Representative full-frame images of wild-type and *Vac14*$^{-/-}$ neurons during baseline (0–10 min), NMDA stimulation (11–15 min) and recovery after wash out (16–55 min). (**B**) Changes in pH-GluA1 fluorescence were calculated from straightened dendrites isolated from full-frame images. (**C**) Wild-type and *Vac14*$^{-/-}$ neurons exhibited similar recovery to baseline levels. (**D**) Average time course for percent change in pH-GluA1 fluorescence, normalized to average baseline intensity. (**E**) Amplitude of change in fluorescence after wash-out of NMDA is decreased in *Vac14*$^{-/-}$ neurons compared to wild type (wild type, 66.72 ± 4.93%; *Vac14*$^{-/-}$ 44.68 ± 7.10%). (**F**) $t_{1/2}$ recycling rate after NMDA removal is normal. *$P = 0.0224$, Two-sample *t*-test, $n = 11$–14. Error bars, s.e.m.

Surface levels of AMPA receptors are tightly controlled by trafficking to and from the cell interior. Consistent with increased mEPSC amplitude, steady-state levels of surface-exposed AMPA receptors are elevated in *Vac14*$^{-/-}$ neurons. Using two independent methods, we found that AMPA receptor internalization following NMDA receptor activation is defective in *Vac14*$^{-/-}$ neurons. The total levels of regulated endocytosed AMPA receptors, quantified from internalized GluA2 puncta or amplitude of change in pHluorin-GluA1 fluorescence, are reduced in *Vac14*$^{-/-}$ neurons, which likely accounts for the elevated surface AMPA receptor levels. This endocytosis defect is consistent with the finding that internalization of transfected GluA2 is reduced in cortical neurons after siRNA knockdown of PIKfyve (Tsuruta *et al*, 2009). Conversely, MTMR2 knockdown, which is predicted to increase PI(3,5)P_2 levels, enhances AMPA receptor endocytosis (Lee *et al*, 2010). Together, these findings suggest a new role for PI(3,5)P_2 and/or PI(5)P, and downstream effector(s), early in the endocytic pathway. Though general endocytosis could be regulated by these signalling lipids, Tsuruta *et al* (2009) found that the internalization of Cav1.2, but not Kv1.2, was affected by PIKfyve knockdown; thus, the PIKfyve/VAC14/FIG4 pathway may play a more selective role in endocytosis of particular membrane proteins.

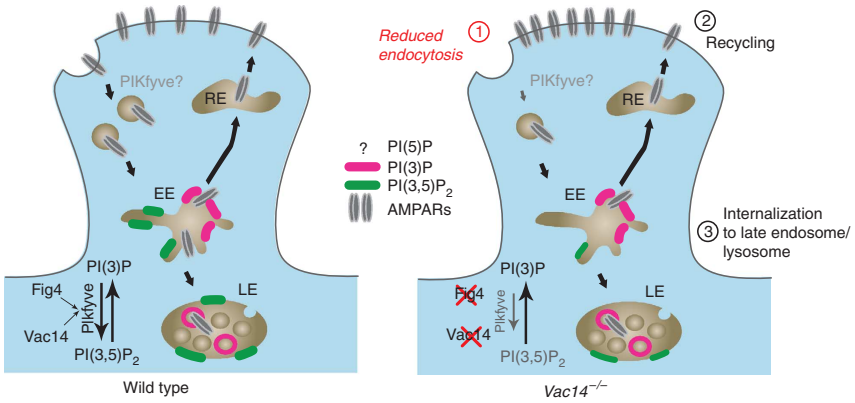

Figure 9 Model of trafficking defects that promote the elevation of surface AMPA receptors in *Vac14*$^{-/-}$ neurons. Endocytosis of surface GluA2 is diminished in *Vac14*$^{-/-}$ neurons compared with wild type (1), while no defects were detected in recycling of internal GluA2 to the cell surface (2) or membrane transport late in the endocytic pathway (3). Note that in the absence of VAC14, FIG4 is destabilized (Lenk *et al*, 2011). EE, early endosomes; LE, late endosomes; RE, recycling endosomes.

While VAC14 is localized throughout the endocytic pathway, we found that the recycling and degradative trafficking of AMPA receptors are normal in *Vac14*$^{-/-}$ neurons. Similarly, EGF receptors traffic normally to lysosomes in *Vac14*$^{-/-}$ fibroblasts (Zhang *et al*, 2007), and EGF receptor trafficking is also unaffected by siRNA knockdown of PIKfyve (Rutherford *et al*, 2006), or overexpression of a dominant-negative mutant PIKfyve (Ikonomov *et al*, 2003), although EGF receptor degradation is slowed when a PIKfyve inhibitor is used (de Lartigue *et al*, 2009). Importantly, since *Vac14*$^{-/-}$ cells have half of the normal levels of PI(3,5)P_2 and PI(5)P, it remains possible that different trafficking steps have distinct sensitivities to the extent of loss of PI(3,5)P_2 and/or PI(5)P. Future work is needed to determine if AMPA receptor trafficking late in the endocytic pathway is affected if the PIKfyve/VAC14/FIG4 pathway is inhibited further.

Potential roles of VAC14 in learning and memory

AMPA receptor expression at synapses is regulated to modify synaptic efficacy in the context of long-term potentiation (LTP) and long-term depression (LTD) (Song and Huganir, 2002), as well as homeostatic control of synaptic function driven by persistent changes in neuronal activity (Turrigiano, 2008). Rab5, which likely acts in pathways that are also regulated by PIKfyve (Jefferies *et al*, 2008), is similarly involved in postsynaptic glutamate receptor trafficking and is required for LTD (Brown *et al*, 2005), raising the possibility that dynamic control of PI(3,5)P_2 and/or PI(5)P synthesis contributes to these forms of synaptic plasticity as well. It is now of interest to assess whether, in addition to the more severe neurophysiological outcomes that accompany PIKfyve/VAC14/FIG4 deficiency, perturbations of the PI(3,5)P_2 and/or PI(5)P-related signalling pathways underlie defects in learning and memory. The *Fig4-I41T* Tg705 transgenic line that survives to 3 months of age with a reduced extent of spongiform degeneration could be useful for this purpose (Lenk *et al*, 2011).

Excitotoxicity in Vac14$^{-/-}$ *neurons*

Excitotoxicity has been implicated in many acute and chronic neurological diseases such as stroke (Rothman and Olney, 1986) and ALS (Beal, 1992; Rothstein *et al*, 1992; Martin, 2010). The increased synaptic efficacy in cultured *Vac14*$^{-/-}$ neurons also raises the question of whether excitotoxicity contributes to the neurodegeneration phenotypes observed in VAC14/FIG4-deficient mouse models. Consistent with this idea, PIKfyve overexpression has been shown to protect cultured neurons against excitotoxicity (Tsuruta *et al*, 2009). In this case, it was postulated that an increase in PIKfyve activity led to downregulation of voltage-gated calcium channels and of GluA2, and possibly other as yet undetermined channels and transporters.

Endogenous VAC14 localizes to multiple compartments in the endomembrane system

A common view in recently published reviews is that PI(3,5)P_2 is confined to late endosomes, and has little overlap with its precursor, PI(3)P, which is thought to be confined to early endosomes. However, in fibroblasts, using an antibody to endogenous VAC14, we found that VAC14 was equally distributed between early and late endosomes as well as lysosomes, with some localization to autophagosomes. Assuming that the location of VAC14 on membranes reflects the distribution of PI(3,5)P_2 and/or PI(5)P, we predict that these lipids may regulate pathways that emanate from each of these organelles. VAC14 also localizes to punctate spots that contain neither EEA1 nor LAMP1, which suggests that there are as yet undetermined organelles that contain PI(3,5)P_2 and PI(5)P. We also found that AMPA receptor internalization and evoked presynaptic vesicle release are altered in the absence of VAC14, which suggests novel roles for PIKfyve/VAC14/FIG4, or their downstream effectors, near the plasma membrane. At present, it remains to be determined whether these effects are specific to neurons or whether the PIKfyve/VAC14/FIG4 pathway regulates selected events near the plasma membrane in other cell types.

In summary, our paper describes a critical new role for VAC14 and, by implication, PI(3,5)P_2 and/or PI(5)P, in regulating synaptic function in neurons. Future work will elucidate specific molecular pathways controlled by PI(3,5)P_2 and/or PI(5)P and may provide insights into the treatment of human neuropathies that can be mitigated via regulation of these lipids. Thus, development of drugs designed to

modulate the levels of these lipids might lead to new therapies for several types of neurological disorders.

Materials and methods

Ethics statement

All animal use was performed in compliance with guidelines of the University Committee on Use and Care of Animals of the University of Michigan and National Institutes of Health.

Electrophysiology

Whole-cell patch clamp recordings were performed with an Axopatch 200B amplifier from 13 to 15 DIV cultured hippocampal pyramidal-like neurons bathed in an extracellular solution containing 119 mM NaCl, 5 mM KCl, 2 mM $CaCl_2$, 2 mM $MgCl_2$, 30 mM glucose, 10 mM HEPES (pH 7.4) plus 1 μM TTX and 10 μM bicuculline to isolate glutamatergic mEPSCs. Internal pipette solution contained 100 mM caesium gluconate, 0.2 mM EGTA, 5 mM $MgCl_2$, 40 mM HEPES, 2 mM Mg-ATP, 0.3 mM Li-GTP, 1 mM QX-314 (pH 7.2). Pipette resistance ranged from 3 to 5 MΩ. Neurons with a pyramidal-like morphology were targeted for analysis. For *Vac14*$^{-/-}$ neurons, pyramidal-like neurons with few to no vacuoles were targeted for analysis. Neurons were voltage clamped at −70 mV, and series resistance was not compensated. mEPSC amplitude and frequency were analysed offline using Minianalysis (Synaptosoft). Average traces and statistical analysis was performed in Matlab (Mathworks). Statistical differences between control and experimental conditions were determined by ANOVA and Tukey-Kramer honestly significant difference (HSD) test.

In order to measure probability of evoked synaptic vesicle release in presynaptic terminals forming synapses onto wild-type or *Vac14*$^{-/-}$ neurons, 24 h after transfection, warm (37°C), 0 Mg^{2+} solution was applied to the bath: 125 mM NaCl, 2.5 mM KCl, 5 mM HEPES, 2 mM $CaCl_2$, 33 mM D-Glucose, pH 7.4). AMPA receptor antagonist, CNQX (20 μM), and $GABA_A$ receptor antagonist, bicuculline (10 μM), were included to isolate NMDA receptor currents. Neurons were voltage clamped at −70 mV and evoked excitatory postsynaptic currents were measured by positioning a stimulating electrode close to the neuron. Once a stable response was obtained, MK801 (20 μM), a use-dependent antagonist for NMDA receptors, was applied to the bath for 5 min without stimulation. Following wash-in, 200 stimulations at 0.33 Hz were delivered in the presence of MK801. The peak of the NMDA receptor current was measured for each and normalized to the first response following MK801 wash-in.

Endocytosis assay

Neurons were treated with 20 μM leupeptin for 30 min before live labelling with mouse GluA2 antibodies diluted in normal medium with leupeptin for 15 min. After washing with neurobasal medium, neurons were incubated in normal medium supplemented with 50 μM NMDA and 20 μM leupeptin for 10 min. Endocytosis was stopped by washing in cold 1 × PBS with 0.1 mM $CaCl_2$ and 1 mM $MgCl_2$. Surface bound GluA2 antibodies were stripped with 0.5 M NaCl/0.2 M acetic acid for 4 min on ice. Neurons were fixed in 2% paraformaldehyde and 2% sucrose for 15 min and permeabilized with 0.1% Triton X-100 for 5 min. After blocking with 2% BSA, neurons were incubated with Alexa 555 anti-mouse secondary antibody for 1 h.

To examine the degradation pathway, neurons were incubated with rat anti-Lamp1 antibodies and then Alexa 488 anti-rat and Alexa 555 anti-mouse secondary antibodies.

Endocytosis and recycling assay

Neurons were transfected at DIV12 by Calcium Phosphate and pHluorin-GluA1 endocytosis and recycling live-imaging assays were performed 36–48 h post transfection. Mattek dishes were placed on the stage of the confocal microscope and perfused with normal extracellular buffer (25 mM HEPES, 120 mM NaCl, 5 mM KCl, 2 mM $CaCl_2$, 2 mM $MgCl_2$, 30 mM D-glucose, 1 mM TTX, pH 7.4). Images were acquired once per minute for (I) a 10 min baseline, (II) after the bath was switched to NMDA stimulation buffer (25 mM HEPES, 120 mM $NaCl_2$, 5 mM KCl, 2 mM $CaCl_2$, 0.2 mM $MgCl_2$, 30 mM D-glucose, 1 mM TTX, 20 mM NMDA, 10 mM glycine, pH 7.4) for 5 min to stimulate internalization, and (III), then following washout of the NMDA stimulation buffer to monitor recycling back to the cell surface. The pHluorin fluorescence was imaged at 488 nm excitation, while mCherry fluorescence was imaged at 559 nm excitation, through a × 60 oil objective at a rate of one image per minute. Images were analysed using ImageJ software (NIH) by straightening the primary dendrite of the neuron, starting from the soma, and calculating the fluorescence intensity relative to the average intensity of the baseline period. The degree of GluA1 endocytosis was determined by analysing the first 1–3 min after NMDA stimulation (max decrease in signal) and the rate of GluA1 recycling was determined by fitting a linear curve to the time after max internalization and calculating the time point at which 50% of fluorescence recovered. pHluorin-GluA1 was a gift of Robert Malinow (Addgene plasmid #24000).

Supplementary data

Supplementary data are available at *The EMBO Journal* Online (http://www.embojournal.org).

Acknowledgements

We thank Dr Silvia Corvera for the EEA1 antibody, Dr John Tesmer for the pMALc2H_{10}T vector, Dr Robert Malinow and Addgene for the pHlorin-GluA1 plasmid, Dr Zhaohui Xu for the Rosetta strain, Cynthia JL Carruthers for conditioned media, Amanda S Perez for help with IMAGE J, Dotty Sorenson for assistance with the EM. We thank the Microscopy Image Analysis Laboratory for technical assistance. This work was supported by NIH grants R01-NS064015 to LSW, RO1-MH085798 to MAS and R01-GM24872 to MHM. AJM was supported in part by NRSA F31NS074740-01 and Neuroscience Training Grant T32EY017878. This work utilized the Microscopy Image Analysis Laboratory of the Michigan Diabetes Research and Training Center funded by K020572 from the National Institute of Diabetes and Digestive and Kidney Diseases.

Author contributions: LSW, MAS, MM, YZ and AJM conceived and designed the experiments. YZ, AJM, SNZ and CJF performed the experiments. YZ, AJM, LSW and MAS analysed the data. LSW, MAS, YZ and AJM wrote the paper.

Conflict of interest

The authors declare that they have no conflict of interest.

References

Balla T (2006) Phosphoinositide-derived messengers in endocrine signaling. *J Endocrinol* **188:** 135–153

Beal MF (1992) Mechanisms of excitotoxicity in neurologic diseases. *FASEB J* **6:** 3338–3344

Bonangelino CJ, Catlett NL, Weisman LS (1997) Vac7p, a novel vacuolar protein, is required for normal vacuole inheritance and morphology. *Mol Cell Biol* **17:** 6847–6858

Bonangelino CJ, Nau JJ, Duex JE, Brinkman M, Wurmser AE, Gary JD, Emr SD, Weisman LS (2002) Osmotic stress-induced increase of phosphatidylinositol 3,5-bisphosphate requires Vac14p, an activator of the lipid kinase Fab1p. *J Cell Biol* **156:** 1015–1028

Brown TC, Tran IC, Backos DS, Esteban JA (2005) NMDA receptor-dependent activation of the small GTPase Rab5 drives the removal of synaptic AMPA receptors during hippocampal LTD. *Neuron* **45:** 81–94

Brunet A, Datta SR, Greenberg ME (2001) Transcription-dependent and -independent control of neuronal survival by the PI3K-Akt signaling pathway. *Curr Opin Neurobiol* **11:** 297–305

Bryant NJ, Piper RC, Weisman LS, Stevens TH (1998) Retrograde traffic out of the yeast vacuole to the TGN occurs via the prevacuolar/endosomal compartment. *J Cell Biol* **142:** 651–663

Cabezas A, Pattni K, Stenmark H (2006) Cloning and subcellular localization of a human phosphatidylinositol 3-phosphate 5-kinase, PIKfyve/Fab1. *Gene* **371:** 34–41

Cantley LC (2002) The phosphoinositide 3-kinase pathway. *Science* **296:** 1655–1657

Chow CY, Landers JE, Bergren SK, Sapp PC, Grant AE, Jones JM, Everett L, Lenk GM, McKenna-Yasek DM, Weisman LS, Figlewicz D, Brown RH, Meisler MH (2009) Deleterious variants of FIG4, a phosphoinositide phosphatase, in patients with ALS. *Am J Hum Genet* **84:** 85–88

Chow CY, Zhang Y, Dowling JJ, Jin N, Adamska M, Shiga K, Szigeti K, Shy ME, Li J, Zhang X, Lupski JR, Weisman LS, Meisler MH (2007) Mutation of FIG4 causes neurodegeneration in the pale tremor mouse and patients with CMT4J. *Nature* **448:** 68–72

Corvera S, D'Arrigo A, Stenmark H (1999) Phosphoinositides in membrane traffic. *Curr Opin Cell Biol* **11:** 460–465

de Lartigue J, Polson H, Feldman M, Shokat K, Tooze SA, Urbé S, Clague MJ (2009) PIKfyve regulation of endosome-linked pathways. *Traffic* **10:** 883–893

Dittman J, Ryan TA (2009) Molecular circuitry of endocytosis at nerve terminals. *Annu Rev Cell Dev Biol* **25:** 133–160

Dong X-p, Shen D, Wang X, Dawson T, Li X, Zhang Q, Cheng X, Zhang Y, Weisman LS, Delling M, Xu H (2010) PI(3,5)P2 controls membrane traffic by direct activation of mucolipin Ca2 + release channels in the endolysosome. *Nat Commun* **1:** 38

Dotti CG, Sullivan CA, Banker GA (1988) The establishment of polarity by hippocampal neurons in culture. *J Neurosci* **8:** 1454–1468

Dove SK, Piper RC, McEwen RK, Yu JW, King MC, Hughes DC, Thuring J, Holmes AB, Cooke FT, Michell RH, Parker PJ, Lemmon MA (2004) Svp1p defines a family of phosphatidylinositol 3,5-bisphosphate effectors. *EMBO J* **23:** 1922–1933

Duex JE, Nau JJ, Kauffman EJ, Weisman LS (2006a) Phosphoinositide 5-phosphatase Fig 4p is required for both acute rise and subsequent fall in stress-induced phosphatidylinositol 3,5-bisphosphate levels. *Eukaryot Cell* **5:** 723–731

Duex JE, Tang F, Weisman LS (2006b) The Vac14p-Fig4p complex acts independently of Vac7p and couples PI3,5P2 synthesis and turnover. *J Cell Biol* **172:** 693–704

Ferguson CJ, Lenk GM, Jones JM, Grant AE, Winters JJ, Dowling JJ, Giger RJ, Meisler MH (2012) Neuronal expression of Fig4 is necessary and sufficient to prevent spongiform neurodegeneration. *Hum Mol Genet* (advance online publication, 6 June 2012; doi:10.1093/hmg/dds179)

Ferguson CJ, Lenk GM, Meisler MH (2009) Defective autophagy in neurons and astrocytes from mice deficient in PI(3,5)P2. *Hum Mol Genet* **18:** 4868–4878

Gary JD, Wurmser AE, Bonangelino CJ, Weisman LS, Emr SD (1998) Fab1p is essential for PtdIns(3)P 5-kinase activity and the maintenance of vacuolar size and membrane homeostasis. *J Cell Biol* **143:** 65–79

Gong L-W, De Camilli P (2008) Regulation of postsynaptic AMPA responses by synaptojanin 1. *Proc Natl Acad Sci USA* **105:** 17561–17566

Han B-K, Emr SD (2011) Phosphoinositide [PI(3,5)P2] lipid-dependent regulation of the general transcriptional regulator Tup1. *Genes Dev* **25:** 984–995

Hirano T, Matsuzawa T, Takegawa K, Sato MH (2011) Loss-of-function and gain-of-function mutations in FAB1A/B impair endomembrane homeostasis, conferring pleiotropic developmental abnormalities in arabidopsis. *Plant Physiol* **155:** 797–807

Hirano T, Sato MH (2011) Arabidopsis FAB1A/B is possibly involved in the recycling of auxin transporters. *Plant Signal Behav* **6:** 583–585

Horton AC, Rácz B, Monson EE, Lin AL, Weinberg RJ, Ehlers MD (2005) Polarized secretory trafficking directs cargo for asymmetric dendrite growth and morphogenesis. *Neuron* **48:** 757–771

Huettner JE, Bean BP (1988) Block of N-methyl-D-aspartate-activated current by the anticonvulsant MK-801: selective binding to open channels. *Proc Natl Acad Sci USA* **85:** 1307–1311

Ibáñez CF (2007) Message in a bottle: long-range retrograde signaling in the nervous system. *Trends Cell Biol* **17:** 519–528

Ikonomov OC, Sbrissa D, Delvecchio K, Xie Y, Jin J-P, Rappolee D, Shisheva A (2011) The phosphoinositide kinase PIKfyve is vital in early embryonic development: Preimplantation lethality of PIKfyve − / − embryos but normality of PIKfyve + / − mice. *J Biol Chem* **286:** 13404–13413

Ikonomov OC, Sbrissa D, Fenner H, Shisheva A (2009) PIKfyve-ArPIKfyve-Sac3 core complex: contact sites and their consequence for Sac3 phosphatase activity and endocytic membrane homeostasis. *J Biol Chem* **284:** 35794–35806

Ikonomov OC, Sbrissa D, Fligger J, Delvecchio K, Shisheva A (2010) ArPIKfyve regulates Sac3 protein abundance and turnover: disruption of the mechanism by Sac3I41T mutation causing Charcot-Marie-Tooth 4J disorder. *J Biol Chem* **285:** 26760–26764

Ikonomov OC, Sbrissa D, Foti M, Carpentier J-L, Shisheva A (2003) PIKfyve controls fluid phase endocytosis but not recycling/degradation of endocytosed receptors or sorting of procathepsin D by regulating multivesicular body morphogenesis. *Mol Biol Cell* **14:** 4581–4591

Ikonomov OC, Sbrissa D, Shisheva A (2001) Mammalian cell morphology and endocytic membrane homeostasis require enzymatically active phosphoinositide 5-kinase PIKfyve. *J Biol Chem* **276:** 26141–26147

Jefferies HBJ, Cooke FT, Jat P, Boucheron C, Koizumi T, Hayakawa M, Kaizawa H, Ohishi T, Workman P, Waterfield MD, Parker PJ (2008) A selective PIKfyve inhibitor blocks PtdIns(3,5)P(2) production and disrupts endomembrane transport and retroviral budding. *EMBO Rep* **9:** 164–170

Jin N, Chow CY, Liu L, Zolov SN, Bronson R, Davisson M, Petersen JL, Zhang Y, Park S, Duex JE, Goldowitz D, Meisler MH, Weisman LS (2008) VAC14 nucleates a protein complex essential for the acute interconversion of PI3P and PI(3,5)P(2) in yeast and mouse. *EMBO J* **27:** 3221–3234

Katona I, Zhang X, Bai Y, Shy ME, Guo J, Yan Q, Hatfield J, Kupsky WJ, Li J (2011) Distinct pathogenic processes between Fig4-deficient motor and sensory neurons. *Eur J Neurosci* **33:** 1401–1410

Kennedy MJ, Ehlers MD (2006) Organelles and trafficking machinery for postsynaptic plasticity. *Annu Rev Neurosci* **29:** 325–362

Kopec CD, Li B, Wei W, Boehm J, Malinow R (2006) Glutamate receptor exocytosis and spine enlargement during chemically induced long-term potentiation. *J Neurosci* **26:** 2000–2009

Lasiecka ZM, Winckler B (2011) Mechanisms of polarized membrane trafficking in neurons - focusing in on endosomes. *Mol Cell Neurosci* **48:** 278–287

Lee HW, Kim Y, Han K, Kim H, Kim E (2010) The phosphoinositide 3-phosphatase MTMR2 interacts with PSD-95 and maintains excitatory synapses by modulating endosomal traffic. *J Neurosci* **30:** 5508–5518

Lemaire J-F, McPherson PS (2006) Binding of Vac14 to neuronal nitric oxide synthase: Characterisation of a new internal PDZ-recognition motif. *FEBS Lett* **580:** 6948–6954

Lenk GM, Ferguson CJ, Chow CY, Jin N, Jones JM, Grant AE, Zolov SN, Winters JJ, Giger RJ, Dowling JJ, Weisman LS, Meisler MH (2011) Pathogenic mechanism of the FIG4 mutation responsible for charcot-marie-tooth disease CMT4J. *PLoS Genet* **7:** e1002104–e1002104

Lu W, Shi Y, Jackson AC, Bjorgan K, During MJ, Sprengel R, Seeburg PH, Nicoll RA (2009) Subunit composition of synaptic AMPA receptors revealed by a single-cell genetic approach. *Neuron* **62:** 254–268

Martin LJ (2010) Mitochondrial and cell death mechanisms in neurodegenerative diseases. *Pharmaceuticals (Basel, Switzerland)* **3:** 839–915

Nicholson G, Lenk GM, Reddel SW, Grant AE, Towne CF, Ferguson CJ, Simpson E, Scheuerle A, Yasick M, Hoffman S, Blouin R, Brandt C, Coppola G, Biesecker LG, Batish SD, Meisler MH (2011) Distinctive genetic and clinical features of CMT4J: a severe neuropathy caused by mutations in the PI(3,5)P2 phosphatase FIG4. *Brain* **134:** 1959–1971

Osborne SL, Wen PJ, Boucheron C, Nguyen HN, Hayakawa M, Kaizawa H, Parker PJ, Vitale N, Meunier FA (2008) PIKfyve negatively regulates exocytosis in neurosecretory cells. *J Biol Chem* **283:** 2804–2813

Rosenmund C, Clements JD, Westbrook GL (1993) Nonuniform probability of glutamate release at a hippocampal synapse. *Science* **262:** 754–757

Roth MG (2004) Phosphoinositides in constitutive membrane traffic. *Physiol Rev* **84:** 699–730

Rothman SM, Olney JW (1986) Glutamate and the pathophysiology of hypoxic–ischemic brain damage. *Ann Neurol* **19:** 105–111

Rothstein JD, Martin LJ, Kuncl RW (1992) Decreased glutamate transport by the brain and spinal cord in amyotrophic lateral sclerosis. *N Engl J Med* **326:** 1464–1468

Rudge SA, Anderson DM, Emr SD (2004) Vacuole size control: regulation of PtdIns(3,5)P2 levels by the vacuole-associated

Vac14-Fig4 complex, a PtdIns(3,5)P2-specific phosphatase. *Mol Biol Cell* **15:** 24–36

Rusten TE, Vaccari T, Lindmo K, Rodahl LMW, Nezis IP, Sem-Jacobsen C, Wendler F, Vincent J-P, Brech A, Bilder D, Stenmark H (2007) ESCRTs and Fab1 regulate distinct steps of autophagy. *Curr Biol* **17:** 1817–1825

Rutherford AC, Traer C, Wassmer T, Pattni K, Bujny MV, Carlton JG, Stenmark H, Cullen PJ (2006) The mammalian phosphatidylinositol 3-phosphate 5-kinase (PIKfyve) regulates endosome-to-TGN retrograde transport. *J Cell Sci* **119:** 3944–3957

Saksena S, Sun J, Chu T, Emr SD (2007) ESCRTing proteins in the endocytic pathway. *Trends Biochem Sci* **32:** 561–573

Sbrissa D, Ikonomov OC, Filios C, Delvecchio K, Shisheva A (2012) Functional dissociation between PIKfyve-synthesized PtdIns5P and PtdIns(3,5)P2 by means of the PIKfyve inhibitor YM201636. *Am J Physiol Cell Physiol* (advance online publication, 23 May 2012; doi:10.1152/ajpcell.00105.2012)

Sbrissa D, Ikonomov OC, Shisheva A (1999) PIKfyve, a mammalian ortholog of yeast Fab1p lipid kinase, synthesizes 5-phosphoinositides. Effect of insulin. *J Biol Chem* **274:** 21589–21597

Shen J, Yu W-M, Brotto M, Scherman JA, Guo C, Stoddard C, Nosek TM, Valdivia HH, Qu C-K (2009) Deficiency of MIP/MTMR14 phosphatase induces a muscle disorder by disrupting Ca(2+) homeostasis. *Nat Cell Biol* **11:** 769–776

Sieburth D, Ch'ng Q, Dybbs M, Tavazoie M, Kennedy S, Wang D, Dupuy D, Rual J-F, Hill DE, Vidal M, Ruvkun G, Kaplan JM (2005) Systematic analysis of genes required for synapse structure and function. *Nature* **436:** 510–517

Song I, Huganir RL (2002) Regulation of AMPA receptors during synaptic plasticity. *Trends Neurosci* **25:** 578–588

Tochio H, Mok YK, Zhang Q, Kan HM, Bredt DS, Zhang M (2000) Formation of nNOS/PSD-95 PDZ dimer requires a preformed beta-finger structure from the nNOS PDZ domain. *J Mol Biol* **303:** 359–370

Tronchère H, Laporte J, Pendaries C, Chaussade C, Liaubet L, Pirola L, Mandel JL, Payrastre B (2004) Production of phosphatidylinositol 5-phosphate by the phosphoinositide 3-phosphatase myotubularin in mammalian cells. *J Biol Chem* **279:** 7304–7312

Tsuruta F, Green EM, Rousset M, Dolmetsch RE (2009) PIKfyve regulates CaV1.2 degradation and prevents excitotoxic cell death. *J Cell Biol* **187:** 279–294

Turrigiano GG (2008) The self-tuning neuron: synaptic scaling of excitatory synapses. *Cell* **135:** 422–435

Yin HL, Janmey PA (2003) Phosphoinositide regulation of the actin cytoskeleton. *Annu Rev Physiol* **65:** 761–789

Zhang X, Chow CY, Sahenk Z, Shy ME, Meisler MH, Li J (2008) Mutation of FIG4 causes a rapidly progressive, asymmetric neuronal degeneration. *Brain* **131:** 1990–2001

Zhang Y, Zolov SN, Chow CY, Slutsky SG, Richardson SC, Piper RC, Yang B, Nau JJ, Westrick RJ, Morrison SJ, Meisler MH, Weisman LS (2007) Loss of Vac14, a regulator of the signalling lipid phosphatidylinositol 3,5-bisphosphate, results in neurodegeneration in mice. *Proc Natl Acad Sci USA* **104:** 17518–17523

